Orchestrated experience-driven Arc/Arg3.1 responses are disrupted in a mouse model of Alzheimer's disease

Published in final edited form as:
Nat Neurosci. 2012 October ; 15(10): 1422–1429. doi:10.1038/nn.3199.

Orchestrated experience-driven *Arc/Arg3.1* responses are disrupted in a mouse model of Alzheimer's disease

Nikita Rudinskiy[1], **Jonathan M. Hawkes**[1,2], **Rebecca A. Betensky**[3], **Megumi Eguchi**[4], **Shun Yamaguchi**[4], **Tara L. Spires-Jones**[1], and **Bradley T. Hyman**[1]

[1]Alzheimer's Disease Research Laboratory, Department of Neurology, MassGeneral Institute for Neurodegenerative Disease, Massachusetts General Hospital, Harvard Medical School, Charlestown, Massachusetts 02129, USA

[2]Behavioral Neuroscience Program, Northeastern University, Boston, Massachusetts 02115, USA

[3]Department of Biostatistics, Harvard School of Public Health, Boston, Massachusetts 02115, USA

[4]Division of Morphological Neuroscience, Gifu University Graduate School of Medicine, Gifu 501–1194, Japan

Abstract

Experience-induced expression of immediate-early gene *Arc/Arg3.1* is known to play a pivotal role in the consolidation of memory. Here we use in-vivo longitudinal multiphoton imaging to show orchestrated activity-dependent expression of *Arc* in the mouse extrastriate visual cortex in response to a structured visual stimulation. In wild-type mice, the amplitude of the *Arc* response in individual neurons strongly predicts the probability of reactivation by a subsequent presentation of the same stimulus. In a mouse model of Alzheimer's disease, this association is markedly disrupted in the cortex specifically near senile plaques. Neurons in the vicinity of plaques are less likely to respond but, paradoxically, there is stronger response in those few neurons around plaques that do respond. To the extent that the orchestrated pattern of *Arc* expression reflects nervous system responses to, and physiological consolidation of, behavioral experience, the disruption in *Arc* patterns reveals plaque-associated interference with neural network integration.

Introduction

Over the last several years a great deal of evidence has emerged for the prominent role of *Arc* in activity-driven synaptic plasticity and long-term memory consolidation (recently reviewed in[1, 2]). *Arc* transcription in principal excitatory neurons is robustly upregulated in relevant cortical networks following sensory experience[3–5]. The product of this gene, Arc, is a postsynaptic protein that participates in dendritic actin remodeling[6] and binds to endocytic machinery to mediate activity-dependent AMPAR scaling[7, 8]. *Arc* knockout mice exhibit an intriguing phenotype with impaired long-term learning while short-term memory is intact[9]. While *Arc* is clearly critical for long term retention of behaviorally relevant experiences, the patterns of expression by which *Arc* activation codes for neural system savings is unknown. Here, we characterize the patterns of *Arc* transcriptional response in visual association cortex to determine how exposure to a stereotyped visual stimulus shapes *Arc* response in each individual neuron to a subsequent exposure to the same stimulus. To tackle this task we

Author contributions

N.R., T.L.S.-J. and B.T.H. designed experiments, analyzed data and wrote the paper. N.R. and J.M.H. performed the experiments. M.E. and S.Y. generated *Arc::dVenus* mice. R.A.B. contributed with statistical analysis of the data.

use *in vivo* multiphoton imaging of *Arc::dVenus* reporter mice overexpressing destabilized version of yellow fluorescent protein Venus under 7.1 kb mouse *Arc* gene promoter[10]. Owing to over 100-fold enrichment in the reporter mRNA over endogenous *Arc* mRNA and comparable mRNA and protein clearance dynamics[10], this reporter strain is well suited to study experience-induced plastic changes in the intact mouse brain using *in vivo* longitudinal microscopy. We found that repeated exposure of mice to the same stimulus led to a remarkable, orchestrated pattern of re-activation of a subset of individual neurons, and that the extent of neuronal activation predicts the extent of neuronal activation at the subsequent exposure to the same stimulus. This suggests that *Arc* encodes a behavioral stimulus through a complex pattern involving numerous neurons, representing in some sense neural system savings of an event.

We then utilized insight into normal patterns of *Arc* activation in the visual association cortex to examine whether or not deficits in neural system integration occur in a model of Alzheimer's disease (AD). Although the classical neuropathological view is that senile plaques, extracellular fibrillar deposits of amyloid-β (Aβ) often accompanied by structural changes including dystrophic neurites and glial activation, are the key cortical lesion in the disease, whether plaques impact neural system function remains controversial. Recent data strongly implicate soluble, oligomeric forms of Aβ as primarily important in disrupting markers of neuronal function including long-term potentiation and behavior[11, 12]. In contrast to these extremes, based on high resolution array tomography structural studies, we have recently proposed a unified theory in which the region in the immediate vicinity of plaques (within ~ 50 μm) is occupied by high concentrations of synaptotoxic soluble oligomeric Aβ[13]. These models have different predictions regarding plaque's relationships to neural system function: if plaques are a local structural lesion, neurons not directly affected by the plaque would function normally; if soluble oligomeric Aβ were freely diffusible and independent of plaques, all neurons in a region that contains Aβ would be functionally impaired; if oligomeric Aβ was present primarily in the immediate vicinity of plaques, neuronal function would be disproportionately affected in that small zone. Since *Arc* responses to stimuli appear to be a stereotyped, complex pattern in which, normally, there is a specific and predictable pattern of *Arc* transcription, we examined whether plaques in a cortical field disrupt this complex pattern, and if so, examined if the pattern of disruption is informative with regard to whether and how plaques impair information processing in the cortex. We found that the presence of amyloid plaques in *APPswe/PS1d9* AD model mice[14] (*APP/PS1*) altered both the likelihood and extent of reactivation of neurons in association cortex following re-exposure to visual stimuli, with predominant effects occurring in the immediate area around individual plaques. These results are consistent with a model in which plaque induced functional alterations are secondary to distributed focal lesions consisting of the plaque and a surrounding halo, which lead to altered neuronal responsiveness to behaviorally relevant stimuli.

Results

Orchestrated Arc::dVenus expression in the visual cortex

To study the characteristics of experience-dependent *Arc* mRNA expression, we employed transgenic mice expressing destabilized Venus (dVenus, which is rapidly degraded to allow imaging of responses over time) under the control of the *Arc* promoter[10]. This reporter faithfully represents activity-dependent *Arc* expression as demonstrated by stimulus-induced mRNA and protein expression dynamics[10] and immunohistochemical (IHC) staining for dVenus and Arc proteins in the brain sections of *Arc::dVenus* mice (Supplementary Fig. 1). Mice were exposed to a visual stimulus similar to that used in [5] and other studies [15, 16]. First, mice were housed in the dark for 60 hours to allow for complete clearance of dVenus expressed in the visual cortex as a result of routine daytime visual experience. Following

light deprivation mice were placed into an illuminated glass cylinder with alternating vertical black and white stripes for 1 hour and then transferred back into the light-proof dark enclosure for 6 hours until imaging (Fig. 1a). The time point of 6 hours was chosen because Arc::dVenus fluorescence in the visual association cortex reaches maximum around 6–8 hours after the end of 1 hour of exposure to light (Supplementary Fig. 2 and [10]). When mice were sacrificed 6 hours after this stimulation and brains processed postmortem by immunohistochemical staining for dVenus protein (Fig. 1b), we observed that this stimulation paradigm led to robust expression of Arc::dVenus in a subset of neurons in the visual cortex, while almost no Arc::dVenus-positive neurons were detected in the same cortical areas following initial light deprivation period (Fig. 1b). Particularly, visual stimulation for 1 hour in the striped cylinder caused Arc::dVenus expression primarily in the layer II/III neurons of the medial areas of extrastriate visual cortex (VISm on Fig. 1b), while the number of Arc::dVenus-positive neurons in the primary visual area (VISp on Fig. 1b) was limited (Supplementary Fig. 3a). At the same time continuous unstructured light stimulation for 7 hours caused more Arc::dVenus expression in the primary visual area and less in the medial extrastriate cortex (Supplementary Fig. 3b).

Arc::dVenus expression 6 hours after stimulation could also be observed in vivo through a cranial window implanted over the visual cortex (Fig. 1c). We observe that a discrete subset of neurons in the layer II/III of extrastriate visual cortex is activated in response to the structured visual stimulus, as seen postmortem (21.6±1.6% of NeuN-positive neurons (mean ±s.d.), Fig. 3b). To test the hypothesis that *Arc* expression reflects neural network's response to experience, after the end of the imaging session we returned mice back into the light-proof enclosure and repeated the stimulation and imaging paradigm (Fig. 1d, 5a). Overall the number of neurons expressing Arc::dVenus (activated neurons) in the second trial was lower than in the first trial (87.5±8.4% of trial 1 (mean±s.d.), Fig. 5b), which is consistent with previous findings[5]. We find that with the second presentation of the identical stimulus, some of the same neurons are reactivated (50.3±3.2% of trial 1, Fig. 5c) and some new neurons are activated (40.9±4.3% of trial 2, Fig. 5d). Intriguingly, the level of Arc::dVenus expression in trial 1 is a significant predictor of neuron reactivation in trial 2. Reactivation probability was approximately 30% for the neurons with lowest detectable Arc::dVenus expression levels and reached 90% for neurons with the highest expression levels (Fig. 6d). When fitted with a Generalized Estimating Equations logistic regression model with accounting for the data clustering within mouse the Arc::dVenus fluorescence intensity in trial 1 was strongly associated with reactivation probability ($p<0.0001$). Moreover, the extent of activation was similar in the two trials with no change (on average) in intensity of each neuron (Fig. 6b). These data indicate that high levels of *Arc* expression change the synaptic properties of neurons to increase their chances of reactivation to subsequent presentations of the same stimulus.

Arc mRNA expression is locally altered by amyloid plaques

To test the hypothesis that Alzheimer-like senile plaque pathology impairs the *Arc* response to physiologically relevant stimuli, we crossed the *Arc::dVenus* mice with *APP/PS1* transgenic mice (*Arc::dVenus*×*APP/PS1*). As the first readout we quantified experience-driven *Arc* promoter activity represented by mean fluorescence intensity of Arc::dVenus-positive neurons. After the first imaging session of mice with plaques (6–7 months of age), we observed a bimodal distribution of expression levels, with *Arc::dVenus*×*APP/PS1* mice having larger proportion of neurons in the second, brighter, modality (Fig. 2c, 2e). This effect contributed to the significant increase of the median of the intensity distribution in *Arc::dVenus*×*APP/PS1* mice compared to their *Arc::dVenus* littermates (Fig. 2d). We did not observe any significant difference between dVenus intensity distributions in 3–4 month

old (preplaque age for *APP/PS1* mice) *Arc::dVenus×APP/PS1* mice compared to non-*APP/PS1* controls (Fig. 2b, 2d).

To estimate potential effects of inflammatory response to the cranial window implantation on the neuronal activation patterns, *Arc::dVenus×APP/PS1* and control *Arc::dVenus* mice were sacrificed 3 weeks after the window implantation and their brains were analyzed postmortem using immunohistochemical staining for microglia and macrophage marker Iba1 (Supplementary Fig. 4a) and activated astrocyte marker GFAP (Supplementary Fig. 4b). Although *Arc::dVenus×APP/PS1* mice clearly had activated microglia and astrocytes associated with amyloid plaques, we detected no overt cortical gliosis linked to the presence of a cranial window in either of genotypes.

To determine the spatial relationship between Arc::dVenus-expressing neurons and amyloid plaques we identified 3-D coordinates of centers of mass of all detected neurons and methoxy-X04-positive plaques in *Arc::dVenus×APP/PS1* datasets. We observed higher Arc::dVenus expression levels in neurons within shorter distance to the closest amyloid plaque (Fig. 2f), indicating that the amyloid plaques locally increase experience-dependent *Arc* promoter activity. We next sought to determine if the presence of an amyloid plaque affects the number of Arc::dVenus-positive neurons in its direct vicinity after stimulation. We found that that the number of activated neurons is reduced in the 20–50 μm vicinity of a methoxy-X04-positive amyloid plaque compared to the same distance from each of randomly placed virtual plaques introduced into neuronal coordinate datasets of *Arc::dVenus×APP/PS1* mice and *Arc::dVenus* control littermates (Fig. 3a). At the same time the number of Arc::dVenus-expressing neurons in the 50–80 μm area was not affected (Fig. 3a). Since the *APP/PS1* model of AD is known to have no significant cortical neuronal loss at this age[17], this finding indicates that the amyloid plaques locally reduce the ability of neurons in their closest proximity to express *Arc* mRNA in response to a stimulus. However, neuronal loss has been reported in the local environment of plaques in a model of AD[17], thus we performed stereological quantification postmortem of neuronal density and the percentage of *Arc* neurons activated in mice sacrificed 6 hours after the end of visual stimulation. Brain sections were immunostained for GFP to visualize Arc::dVenus and for pan-neuronal marker NeuN (Fig. 3d). We counted the proportion of Arc::dVenus-positive neurons in layer II/III of medial extrastriate visual cortex in the areas immediately adjacent to the plaques and far away from the plaque. The proportion of NeuN-positive neurons with Arc::dVenus expression in control brain was 21.6±1.6%. In *Arc::dVenus×APP/PS1* brain, 24.3±2.06% of neurons far from plaques had Arc::dVenus expression, while only 10.7±0.67% of neurons had *Arc* activation near plaques $P < 0.01$, Fig. 3b). In the same 20–50 μm region around a plaque where we observed a decrease in *Arc* activation, we did not observe any significant neuronal loss as evidenced by maintenance of NeuN density (Fig. 3c and 3d). The only detectable loss of NeuN-positive cells was in the immediate vicinity of plaques (5–10 μm from the plaque edge, data not shown).

We observed another interesting effect of plaques on *Arc* activation in local neurites. Dystrophic swelling of neurites are commonly present next to amyloid plaques both in human AD brain[18] and amyloid plaque-bearing mouse models including *APP/PS1*[19] but their functional role in the disease pathogenesis is unknown. Abnormally swollen plaque-associated axons and dendrites represent only a small fraction of total neuropil, but when neurons of plaque-bearing mice are transgenically modified to express a fluorescent protein either by crossing with a reporter strain or by using a gene delivery vector, the dystrophies belonging to the modified neurons accumulate the fluorescent protein and can be easily visualized[20–22]. Surprisingly, in *Arc::dVenus×APP/PS1* mice we never observed a single dVenus-filled neuritic dystrophy (over 300 total methoxy-X04-positive amyloid plaques imaged in 16 mice, Fig. 4a, rightmost panel), while the YFP-positive dystrophies were

present, in *APP/PS1* mice crossed with YFP (*Thy1::YFP×APP/PS1* strain) as expected[20, 22] (arrowheads, Fig. 4a, leftmost panel) as well as in *APP/PS1* mice expressing GFP in the layer II/III of the visual cortex after stereotaxic injection of AAV2/1-CBA::GFP virus (Fig. 4a, middle panel). Since Thy1::YFP, CBA::GFP and Arc::dVenus are all expressed in cortical pyramidal neurons which usually have abundant dystrophic neurites, this would imply that the neurons with neuritic dystrophies were not able to activate *Arc* promoter in response to the relevant stimulus. To confirm that dystrophic neurites are present around amyloid plaques in *Arc::dVenus×APP/PS1* brains, we performed immunohistochemical analysis of brain sections of *Arc::dVenus×APP/PS1* mice sacrificed 6 hours after the end of stimulation. Indeed, axonal dystrophies visualized with SMI-312 antibody (arrowheads, Fig. 4b) and dendritic dystrophies visualized with SMI-32 (arrowheads, Fig. 4c) were present around plaques in *Arc::dVenus* mice but they did not contain dVenus despite activation of nearby neurites in response to stimulation.

These data indicate that amyloid plaques are associated with the opposing effects of reducing the proportions of neurons that express *Arc* in response to a stimulus in the vicinity of plaques and eliminating the ability of neurons with plaque-associated dystrophies in their neurites to respond to stimulation, while the few neurons near plaques that do respond appear hyperactive with an increased level of *Arc* expression.

Coordinated *Arc* expression is disrupted in *APP/PS1* mice

To assess the effect of Aβ pathology on *Arc* response to repeated presentation of the same stimulus which the mice should have a memory of, we monitored activation status and Arc::dVenus expression levels in cortical neurons in two consecutive stimulation trials (Fig. 1d, 5a). The number of activated neurons in the second trial in *Arc::dVenus×APP/PS1* mice was similar to that observed in control mice, which decreased compared to the first trial as observed in control littermates (68.4±5.3% of trial 1 (mean±s.d.), Fig. 5b). The percentage of trial 1 neurons that were reactivated in the trial 2 (45.0±3.0% of trial 1) and the percentage of newly activated neurons in trial 2 (33.6±3.1% of trial 2) was not significantly affected by *APP/PS1* genotype either (Fig. 5c and 5d). At the same time the proportion of neurons that had a higher level of Arc::dVenus expression in the trial 2 was smaller in *Arc::dVenus×APP/PS1* mice compared to the control littermates (35.1±3.4% of trial 1 in APP/PS vs. 47.7±2.6 % in controls, Fig. 5e). Notably, *APP/PS1* genotype had a significant effect only on Arc::dVenus expression levels (measured in trial 1) in the neuronal population that was activated in both trials (Fig. 5f), but not in populations that were either activated only in trial 1 or only in trial 2 (Fig. 5g and 5h).

To better demonstrate the differences in patterns of Arc::dVenus expression changes we created a spaghetti plot where each line connecting every neuron's intensities in trials 1 and 2 is color-coded according to the absolute change of intensity (Fig. 6a). This plot highlights the fact that in *Arc::dVenus×APP/PS1* mice, a large population of neurons with abnormally high levels of expression in trial 1 is reactivated in trial 2 with much lower expression levels, while there are very few neurons that experience the opposite change of activity–from low to high. In the control littermates these two populations are balanced and the distribution of Arc::dVenus intensity change from trial 1 to trial 2 looks symmetrical with the median around 0 arbitrary units (AU, Fig. 6b, top panel; Fig. 6e). The distribution of the intensity change in *Arc::dVenus×APP/PS1* mice is skewed to the left indicating that majority of reactivated neurons had lower expression levels in trial 2 (Fig. 6b, bottom panel; Fig. 6e). After normalization to the trial 1 expression levels, relative intensity change in *Arc::dVenus×APP/PS1* mice was significantly shifted into the negative side (Fig. 6c, 6f).

The association of *Arc* expression level in trial 1 with reactivation probability in trial 2 observed in control mice was significantly reduced in *Arc::dVenus×APP/PS1* mice. In

Arc::dVenus×APP/PS1 mice the log odds of reactivation were decreased by 0.59 compared to controls after adjustment for trial 1 intensity ($p<0.01$). The solid lines on Fig. 6d represent model-based probabilities plotted as a function of intensity separately for *Arc::dVenus×APP/PS1* mice and control littermates. This loss of correlation between the level of activation at first presentation and reactivation at the second presentation could represent a failure of the *APP/PS1* brain to change synaptic properties in response to *Arc* activation thus contributing to disrupted memory consolidation.

Discussion

Here we take advantage of a mouse model expressing destabilized Venus under the control of the *Arc* promoter combined with longitudinal multiphoton imaging in living mice to study the activity-dependent expression of *Arc* in visual circuits in response to physiologically relevant, complex stimulation. We find in control brain that there is robust activation of *Arc* promoter in neurons of medial extrastriate visual cortex in response to a structured visual stimulation and that the probability of neuronal activation is tightly correlated with the *Arc* expression level following previous exposure to the same stimulus. The characteristic patterns of *Arc* responses were found to be altered by cerebral amyloid plaque deposition. In contrast to wild type animals, in the visual cortex of amyloid plaque-bearing AD model mice we observe: (**a**) the proportion of *Arc* responsive neurons is strongly decreased in the closest vicinity of plaques; (**b**) at the same time, a small population of cortical neurons express *Arc* mRNA in response to a sensory experience at abnormally high levels, especially within the same small region surrounding plaques; (**c**) neurons with plaque-associated neuritic dystrophies do not express *Arc* mRNA in response to a stimulus; (**d**) the correlation between level of *Arc* activation at the first stimulus and the probability of reactivation with a subsequent presentation is weakened by amyloid plaque pathology. Together these data support a model in which plaques disrupt the normal integrative functions of the cortex in their immediate microenvironment.

Arc is strongly implicated in memory consolidation and synaptic changes[9, 23, 24]. Coordinated levels of *Arc* expression are extremely important for correct execution of synaptic plasticity underlying encoding of long-term changes, via mechanisms including regulation of AMPAR endocytosis[8] and promotion of F-actin polymerization[6]. Thus mice with *Arc* knock-down exhibit impaired long-term synaptic consolidation in various behavioral tasks[9, 24] and *Arc* overexpression leads to a decrease in surface AMPARs[8] and reduces AMPAR-mediated synaptic transmission[25]. Our data showing a positive correlation between neuronal activation in response to a stimulus and levels of *Arc* expression following subsequent exposure to a similar stimulus suggest that one role of *Arc* in memory consolidation is to strengthen responses to stimuli in cells with high levels of *Arc* after the first stimulus presentation. This highlights the importance of precise regulation of *Arc* promoter activity for normal neurophysiology.

Our findings are consistent with the well established association of Aβ deposition and soluble Aβ with memory and plasticity deficits, synapse loss and neuritic structural changes (reviewed in [26]). Our current results show that abnormal hyper- and hypo-active behavior of viable neurons in AD brain extends to higher-order functions such as the long-lasting consolidation of synaptic connections mediated by Arc, and that these effects are predominantly found in the immediate vicinity of plaques. These results highlight the same microanatomical areas we have previously demonstrated using structural tools to contain high concentrations of oligomeric Aβ[13]. These results are also in broad concert with observations using calcium imaging in living mice which showed clusters of neurons[27] and neurites[28] with calcium overload in anesthetized mouse cortex in close proximity of amyloid

plaques, extending those observations to the level of neural circuit integration in awake, behaving animals.

These findings also shed light on a controversial literature as to whether *Arc* is up- or down-regulated in the brain in Alzheimer models and in Alzheimer's disease itself. For example, AD-related pathology is linked with an increase in *Arc* expression in 6 studies[29–34], a decrease in 9 studies[34–43], and no change in 3 studies[44–46] (summarized in Supplementary Table 1). These discrepancies could be due to artifacts of *in vitro* systems or the static nature of post-mortem experiments which do not allow analysis of *Arc* dynamics, nor the analysis of *Arc* in the context of specific behavioral stimuli. Here, with our longitudinal imaging in vivo, we observe that amyloid plaques act locally to aberrantly increase *Arc* promoter activity in the responsive neurons, but the proportion of activated neurons in the direct vicinity of plaques is decreased. Moreover, neurons that had amyloid plaque-associated dystrophic neurites were not able to express *Arc* mRNA, a fact that indicates the possibility that an amyloid plaque can affect functional properties of neurons with somata located relatively far away. One might argue that the observed plaque-associated functional impairments affect only a small proportion of neurons. In fact, when we take into account the extent of amyloid deposition in the brains of AD patients, a 50 μm vicinity of Aβ plaque containing functionally defective neurons would represent at least 70% of total affected cortical volume(conservative estimate based on temporal lobe data from [47]).

Multiple recent lines of evidence suggest that cognitive deficits in early AD are due to large-scale neuronal network dysfunction, although the extent to which this is mediated by Aβ plaques as opposed to associated tangles, neuronal loss, or even soluble forms of amyloid is uncertain (e.g. reviewed in [48]). Patients with AD exhibit regional hypometabolism and disrupted whole-brain activation patterns[49], while pre-symptomatic AD patients[50], characterized by amyloid deposits noted on neuroimaging, exhibit abnormal functional hyperactivity during memory encoding tasks. Overall, our results in a mouse model that develops senile plaques (but no neurofibrillary tangles or overt neuronal loss) in the cortex suggest that amyloid deposits and surrounding soluble Aβ introduce complex aberrations into the coordinated execution of activity-dependent transcriptional programs in excitatory neurons, which we hypothesize at least partially underlie the abnormalities in neural system function noted even before clinical symptoms in AD.

Materials and Methods

Mice and surgery

Arc::dVenus mice overexpressing destabilized Venus under 7.1 kb mouse *Arc* promoter[10] (C57BL/6J background) were crossed with $APP_{SWE;}PS1dE9$ mice[14] (*APP/PS1* in the text). *Arc::dVenus*-positive non-carriers of *APP/PS1* transgene were used as controls for this study. Mice had cranial windows implanted as described previously[21] over the right visual cortical area at least 3 weeks before imaging to allow for recovery from surgical trauma. Anesthesia used for cranial window implantation was induced with 4% isoflurane in balanced oxygen and maintained at the level of 1.2–1.6% during the surgery. Body temperature was maintained at 37°C.

Brain tissue from *Thy1::YFP×APP/PS1* mice was acquired from a previous study[22]. Briefly, *Thy1::YFP×APP/PS1* mice were perfused with 4% paraformaldehyde and 0.1% glutaraldehyde fixative and coronal sections of 50 μm obtained through the brain. All mice used in the study were 6–7 months old, except for the pre-plaque *Arc::dVenus×APP/PS1* cohort and their control littermates, which were 3–3.5 months old. All animal experimentation was performed in conformance with institutional and NIH guidelines and approved by the MGH Institutional Animal Care and Use Committee.

To express GFP in the layer II/III neurons of the visual cortex, *APP/PS1* mice were stereotaxically injected with AAV2/1-CBA::GFP virus (MassGeneral Vector core) during window implantation. 3 weeks were allowed for the transgene expression and recovery from the surgical trauma prior to imaging.

Visual stimulation and *in vivo* multiphoton imaging

Prior to each visual stimulation mice were given an IP injection of amyloid-plaque labeling agent methoxy-XO4 (5 mg/kg)[20] and placed for 60 hours in their home cages into the dark light-proof ventilated cardboard enclosures accommodating one cage each. After the end of light deprivation period mice were transferred to a glass cylinder (30 cm tall, 20 cm wide) with alternating vertical black and white stripes (2 cm wide) applied to the wall. The cylinder was illuminated from the outside, yielding illuminance of approximately 200 lux inside of the cylinder. Following visual stimulation mice were transferred back to their home cages and placed into dark, light-proof enclosures for 6 hours until imaging. Anesthesia was induced inside the light-proof enclosure with 4% isoflurane, mice were transferred to custom-made imaging stage and anesthesia maintained at the level of ~ 1.5%. Texas Red-conjugated dextran (MW 70,000Da, 12.5mg/mL in sterile PBS, Molecular Probes) was injected IV to provide fluorescent angiogram used to locate the same brain region in consecutive imaging sessions and to be used as a reference fluorophore for the control of cranial window quality. Imaging was performed on Olympus Fluoview 1000 MPE system coupled with Olympus BX61WI upright microscope with XLPLN 25x water-immersion objective (NA = 1.05). Excitation light was produced by a mode-locked titanium/sapphire MaiTai laser (Spectra-Physics) tuned to 860 mm with the output power set to 100 mW. Emitted light was collected in three channels: 460–500 nm (amyloid-bound methoxy-X04), 530–560 nm (dVenus fluorescence) and 575–630 nm (Texas Red dextran angiogram). Z-stacks were acquired with the resolution of 1 μm/pixel in X-Y dimension with the Z-step of 3 μm. For each mouse imaged site consisted of 2×4 512×512×240 μm stacks acquired with 10% overlap in X–Y dimensions resulting in an imaged field in visual cortex spanning roughly 1×2×0.24 mm^3 ((m−l)×(r−c)×(d−v)),. Imaging settings were kept constant in all imaging sessions. For time course imaging (Supplementary Fig. 2) mice where anesthetized for the duration of imaging (~ 20 min) at each given time point after the end of visual stimulation and returned into the light deprivation box until the next time point. Mice with visible bleeding or infection under cranial window were excluded from the study, as well as the mice with vascularized tissue overgrowth (visualized with Texas Red dextran angiogram) under cranial window (approx. 40% of total mice). For the remaining mice, quality and stability of the cranial windows were assessed after each imaging session by (a) examining z-profile of Texas Red dextran fluorescent signal and (b) examining neuronal *Arc::dVenus* expression level distributions (see Fig. 2b, 2c), since any changes in window clarity would significantly shift modal values and interquartile ranges of these distributions. Mice with abnormally low absolute Texas Red signal levels were excluded from the study (approx. 10% of the remaining mice). Postmortem examination of mice with windows deemed stable revealed no tissue growth between the cranial window and the brain surface, and no overt cortical inflammatory response was detected (see Supplementary Fig. 4). Additionally, z-profiles of Texas Red dextran-filled blood vessels from consecutive imaging sessions of the same mice were compared to each other to exclude possible window clouding between the sessions. No mice were disqualified from the study based on this examination. For the illustration of response “before” and “after” stimulation in Fig. 1c and Fig. 2a, mice were first placed into 60-hour light deprivation, stimulated in a striped cylinder as described above and imaged (time point “after” stimulation). Then they were allowed to recover from anesthesia, returned to the dark light-proof enclosure for another 60 hours and imaged again (time point “before” stimulation). Overview *in vivo* images for Supplementary Fig. 1 were obtained on an upright Olympus BX50WI microscope fitted with XLFluor 2x/

340 objective with NA=0.14, YFP filter cube (ex/em: 500/545 nm), and using short arc mercury lamp as the excitation light source.

Image processing

All image processing was performed using Fiji package of NIH ImageJ software (fiji.sc; rsbweb.nih.gov/ij). Overlapping 3-D-stacks were stitched based on the angiogram channel using "3D Stitching" plug-in[51]. Background was subtracted and median filter applied. For quantification of *Arc::dVenus* expression levels, stitched stacks were z-projected and mean fluorescent signal in each individually detected cell body was measured. To determine 3d coordinates of amyloid plaques and neuronal cell bodies 3d stacks were segmented using "3D Object Counter" plug-in. When counting number of *Arc::dVenus*-positive neurons at different distances from plaques, we excluded from analysis real and virtual plaques that had no neurons in 100 μm radius (this criterion eliminated from the analysis roughly 40% of real and virtual plaques) since the *Arc::dVenus*-positive neurons are not distributed evenly across each dataset unlike the methoxy-X04-positive amyloid plaques.

Post-mortem tissue analysis

To obtain tissue for immunohistochemistry animals were transcardially perfused with ice-cold phosphate-buffered saline (PBS) followed by 4% paraformaldehyde in PBS. Brains were incubated in fixative at 4°C for additional 48 hours. 50 μm free-floating sections were cut on a Microm HM400 microtome. Following primary antibodies were used: chicken anti-GFP (1:500, Cat. No GFP-1020, Aves Labs); mouse SMI-312 (1:500, Cat. No SMI-312R, Covance); mouse SMI-32 (1:500, Cat. No SMI-32R, Covance, NJ); mouse NeuN (1:500, Cat. No MAB377, Millipore); mouse anti-Arc (1:1000, Cat. No sc-17839, Santa Cruz); rabbit Iba1 (1:500, Wako, Cat. No 019-19741). Secondary antibodies used were: goat-anti-chicken AlexaFluor488 (1:500, Cat. No A-11039, Molecular Probes); goat-anti-mouse Cy3 (1:500, Cat. No 115-165-166, Jackson ImmunoResearch); goat-anti-rabbit (1:500, Cat. No 111-165-144, Jackson ImmunoResearch). High resolution images for Figure 4 were acquired on a Zeiss LSM 510 META confocal microscope equipped with two-photon Coherent Chameleon laser and presented here as Z-projections. Overview low resolution images for Figure 1 were acquired on Zeiss Axio Observer.Z1 fluorescent microscope and aligned to Allen Brain reference atlas (brain-map.org). IHC images for Supplementary Fig. 1 and 4 were acquired on Zeiss Axio Observer.Z1. Stereological counting of *Arc::dVenus*-and NeuN-positive neurons was performed on Olympus CAST system in neuronal layer II/III of medial extrastriate visual cortex of mice that had not undergone window implantation and *in vivo* imaging. To define a region "near plaque" the edge of stereological counting frame (65×65 μm) was placed at a distance of 10 μm from a plaque's center. Regions "far from plaque" were selected randomly with the condition that no plaque was present within at least 50 μm from the edge of the counting frame.

Statistical analysis

The normality of all datasets was tested using Kolmogorov-Smirnov method. Multiple comparisons of non-normal data was performed using Kruskal-Wallis method with Dunn's post-test for pair-wise comparison. Multiple comparisons of normal data was performed using one-way or repeated measures two-way (when indicated) ANOVA with Bonferroni post-test for pair-wise comparison of mean values across mice. Simple comparison of two sets of normal data across mice was performed using unpaired Student's t-test. Mann-Whitney test was used to compare two sets of non-normal data. Non-normal distributions of fluorescence intensity levels in *Arc::dVenus* neurons were compared using Wilcoxon rank-sum test with correction for clustering of values within individual mice. The association of *Arc::dVenus* intensity with reactivation probability (Fig. 6d) was tested by fitting a Generalized Estimating Equations logistic regression model using an independent working

correlation matrix (accounting for the data clustering within mouse), implemented in SAS Version 9.3. All reported p-values are two-tailed.

Supplementary Material

Refer to Web version on PubMed Central for supplementary material.

Acknowledgments

We thank A. Muzikansky (Harvard), B. Urbanc and B. Cohen (Drexel) for their help with statistical analysis. We also thank all the members of the Hyman laboratory for their input, discussions and help with the equipment. N.R. is supported by the fellowships from the Swiss National Science Foundation and the Swiss Foundation for Grants in Biology and Medicine. This research is supported by a gift from the Gilbert fund, grants from the US National Institutes of Health (AG033670 to T.L.S-J. and AG08487 to B.T.H.) and a grant from the Harvard Neuro Discovery Center to R. A. B.

References

1. Shepherd JD, Bear MF. New views of Arc, a master regulator of synaptic plasticity. Nat Neurosci. 2011; 14:279–284. [PubMed: 21278731]
2. Korb E, Finkbeiner S. Arc in synaptic plasticity: from gene to behavior. Trends in neurosciences. 2011; 34:591–598. [PubMed: 21963089]
3. Ramirez-Amaya V, et al. Spatial exploration-induced Arc mRNA and protein expression: evidence for selective, network-specific reactivation. J Neurosci. 2005; 25:1761–1768. [PubMed: 15716412]
4. Tagawa Y, Kanold PO, Majdan M, Shatz CJ. Multiple periods of functional ocular dominance plasticity in mouse visual cortex. Nat Neurosci. 2005; 8:380–388. [PubMed: 15723060]
5. Wang KH, et al. In vivo two-photon imaging reveals a role of arc in enhancing orientation specificity in visual cortex. Cell. 2006; 126:389–402. [PubMed: 16873068]
6. Messaoudi E, et al. Sustained *Arc/Arg3.1* synthesis controls long-term potentiation consolidation through regulation of local actin polymerization in the dentate gyrus in vivo. J Neurosci. 2007; 27:10445–10455. [PubMed: 17898216]
7. Chowdhury S, et al. *Arc/Arg3.1* interacts with the endocytic machinery to regulate AMPA receptor trafficking. Neuron. 2006; 52:445–459. [PubMed: 17088211]
8. Shepherd JD, et al. *Arc/Arg3.1* mediates homeostatic synaptic scaling of AMPA receptors. Neuron. 2006; 52:475–484. [PubMed: 17088213]
9. Plath N, et al. *Arc/Arg3.1* is essential for the consolidation of synaptic plasticity and memories. Neuron. 2006; 52:437–444. [PubMed: 17088210]
10. Eguchi M, Yamaguchi S. In vivo and in vitro visualization of gene expression dynamics over extensive areas of the brain. Neuroimage. 2009; 44:1274–1283. [PubMed: 19059347]
11. Cleary JP, et al. Natural oligomers of the amyloid-beta protein specifically disrupt cognitive function. Nat Neurosci. 2005; 8:79–84. [PubMed: 15608634]
12. Shankar GM, et al. Amyloid-beta protein dimers isolated directly from Alzheimer's brains impair synaptic plasticity and memory. Nature medicine. 2008; 14:837–842.
13. Koffie RM, et al. Oligomeric amyloid beta associates with postsynaptic densities and correlates with excitatory synapse loss near senile plaques. Proceedings of the National Academy of Sciences of the United States of America. 2009; 106:4012–4017. [PubMed: 19228947]
14. Jankowsky JL, et al. Co-expression of multiple transgenes in mouse CNS: a comparison of strategies. Biomolecular engineering. 2001; 17:157–165. [PubMed: 11337275]
15. Blakemore C, Cooper GF. Modification of the visual cortex by experience. Brain research. 1971; 31:366. [PubMed: 5569159]
16. Sengpiel F, Stawinski P, Bonhoeffer T. Influence of experience on orientation maps in cat visual cortex. Nat Neurosci. 1999; 2:727–732. [PubMed: 10412062]
17. Urbanc B, et al. Neurotoxic effects of thioflavin S-positive amyloid deposits in transgenic mice and Alzheimer's disease. Proceedings of the National Academy of Sciences of the United States of America. 2002; 99:13990–13995. [PubMed: 12374847]

18. Dickson TC, Vickers JC. The morphological phenotype of beta-amyloid plaques and associated neuritic changes in Alzheimer's disease. Neuroscience. 2001; 105:99–107. [PubMed: 11483304]
19. Jankowsky JL, Xu G, Fromholt D, Gonzales V, Borchelt DR. Environmental enrichment exacerbates amyloid plaque formation in a transgenic mouse model of Alzheimer disease. Journal of neuropathology and experimental neurology. 2003; 62:1220–1227. [PubMed: 14692698]
20. Meyer-Luehmann M, et al. Rapid appearance and local toxicity of amyloid-beta plaques in a mouse model of Alzheimer's disease. Nature. 2008; 451:720–724. [PubMed: 18256671]
21. Spires TL, et al. Dendritic spine abnormalities in amyloid precursor protein transgenic mice demonstrated by gene transfer and intravital multiphoton microscopy. J Neurosci. 2005; 25:7278–7287. [PubMed: 16079410]
22. Rozkalne A, Hyman BT, Spires-Jones TL. Calcineurin inhibition with FK506 ameliorates dendritic spine density deficits in plaque-bearing Alzheimer model mice. Neurobiol Dis. 2011; 41:650–654. [PubMed: 21134458]
23. Maddox SA, Schafe GE. The activity-regulated cytoskeletal-associated protein (*Arc/Arg3.1*) is required for reconsolidation of a Pavlovian fear memory. J Neurosci. 2011; 31:7073–7082. [PubMed: 21562269]
24. Guzowski JF, et al. Inhibition of activity-dependent arc protein expression in the rat hippocampus impairs the maintenance of long-term potentiation and the consolidation of long-term memory. J Neurosci. 2000; 20:3993–4001. [PubMed: 10818134]
25. Rial Verde EM, Lee-Osbourne J, Worley PF, Malinow R, Cline HT. Increased expression of the immediate-early gene *Arc/Arg3.1* reduces AMPA receptor-mediated synaptic transmission. Neuron. 2006; 52:461–474. [PubMed: 17088212]
26. Koffie RM, Hyman BT, Spires-Jones TL. Alzheimer's disease: synapses gone cold. Molecular neurodegeneration. 2011; 6:63. [PubMed: 21871088]
27. Busche MA, et al. Clusters of hyperactive neurons near amyloid plaques in a mouse model of Alzheimer's disease. Science. 2008; 321:1686–1689. [PubMed: 18802001]
28. Kuchibhotla KV, et al. Abeta plaques lead to aberrant regulation of calcium homeostasis in vivo resulting in structural and functional disruption of neuronal networks. Neuron. 2008; 59:214–225. [PubMed: 18667150]
29. Grinevich V, et al. Fluorescent *Arc/Arg3.1* indicator mice: a versatile tool to study brain activity changes in vitro and in vivo. J Neurosci Methods. 2009; 184:25–36. [PubMed: 19628007]
30. Lacor PN, et al. Synaptic targeting by Alzheimer's-related amyloid beta oligomers. J Neurosci. 2004; 24:10191–10200. [PubMed: 15537891]
31. Perez-Cruz C, et al. Reduced spine density in specific regions of CA1 pyramidal neurons in two transgenic mouse models of Alzheimer's disease. J Neurosci. 2011; 31:3926–3934. [PubMed: 21389247]
32. Rosi S, et al. Neuroinflammation alters the hippocampal pattern of behaviorally induced Arc expression. J Neurosci. 2005; 25:723–731. [PubMed: 15659610]
33. Wu J, et al. *Arc/Arg3.1* regulates an endosomal pathway essential for activity-dependent beta-amyloid generation. Cell. 2011; 147:615–628. [PubMed: 22036569]
34. Palop JJ, et al. Aberrant excitatory neuronal activity and compensatory remodeling of inhibitory hippocampal circuits in mouse models of Alzheimer's disease. Neuron. 2007; 55:697–711. [PubMed: 17785178]
35. Chen TJ, Wang DC, Chen SS. Amyloid-beta interrupts the PI3K-Akt-mTOR signaling pathway that could be involved in brain-derived neurotrophic factor-induced Arc expression in rat cortical neurons. J Neurosci Res. 2009; 87:2297–2307. [PubMed: 19301428]
36. Dickey CA, et al. Amyloid suppresses induction of genes critical for memory consolidation in APP + PS1 transgenic mice. J Neurochem. 2004; 88:434–442. [PubMed: 14690531]
37. Dickey CA, et al. Selectively reduced expression of synaptic plasticity-related genes in amyloid precursor protein+ presenilin-1 transgenic mice. J Neurosci. 2003; 23:5219–5226. [PubMed: 12832546]
38. Echeverria V, Berman DE, Arancio O. Oligomers of beta-amyloid peptide inhibit BDNF-induced arc expression in cultured cortical Neurons. Curr Alzheimer Res. 2007; 4:518–521. [PubMed: 18220514]

39. Fox LM, et al. Soluble tau species, not neurofibrillary aggregates, disrupt neural system integration in a tau transgenic model. Journal of neuropathology and experimental neurology. 2011; 70:588–595. [PubMed: 21666499]
40. Ginsberg SD, Hemby SE, Lee VM, Eberwine JH, Trojanowski JQ. Expression profile of transcripts in Alzheimer's disease tangle-bearing CA1 neurons. Ann Neurol. 2000; 48:77–87. [PubMed: 10894219]
41. Palop JJ, et al. Vulnerability of dentate granule cells to disruption of arc expression in human amyloid precursor protein transgenic mice. J Neurosci. 2005; 25:9686–9693. [PubMed: 16237173]
42. Wang DC, Chen SS, Lee YC, Chen TJ. Amyloid-beta at sublethal level impairs BDNF-induced arc expression in cortical neurons. Neurosci Lett. 2006; 398:78–82. [PubMed: 16412575]
43. Wegenast-Braun BM, et al. Independent effects of intra-and extracellular Abeta on learning-related gene expression. The American journal of pathology. 2009; 175:271–282. [PubMed: 19556514]
44. Chin J, et al. Fyn kinase induces synaptic and cognitive impairments in a transgenic mouse model of Alzheimer's disease. J Neurosci. 2005; 25:9694–9703. [PubMed: 16237174]
45. Cuadrado-Tejedor M, et al. Sildenafil restores cognitive function without affecting beta-amyloid burden in a mouse model of Alzheimer's disease. British journal of pharmacology. 2011; 164:2029–2041. [PubMed: 21627640]
46. Herring A, et al. Exercise during pregnancy mitigates Alzheimer-like pathology in mouse offspring. The FASEB journal : official publication of the Federation of American Societies for Experimental Biology. 2012; 26:117–128.
47. Hyman BT, et al. Quantitative analysis of senile plaques in Alzheimer disease: observation of log-normal size distribution and molecular epidemiology of differences associated with apolipoprotein E genotype and trisomy 21 (Down syndrome). Proceedings of the National Academy of Sciences of the United States of America. 1995; 92:3586–3590. [PubMed: 7724603]
48. Palop JJ, Mucke L. Amyloid-beta-induced neuronal dysfunction in Alzheimer's disease: from synapses toward neural networks. Nat Neurosci. 2010; 13:812–818. [PubMed: 20581818]
49. Drzezga A, et al. Neuronal dysfunction and disconnection of cortical hubs in non-demented subjects with elevated amyloid burden. Brain : a journal of neurology. 2011; 134:1635–1646. [PubMed: 21490054]
50. Sperling RA, et al. Amyloid deposition is associated with impaired default network function in older persons without dementia. Neuron. 2009; 63:178–188. [PubMed: 19640477]
51. Preibisch S, Saalfeld S, Tomancak P. Globally optimal stitching of tiled 3D microscopic image acquisitions. Bioinformatics. 2009; 25:1463–1465. [PubMed: 19346324]

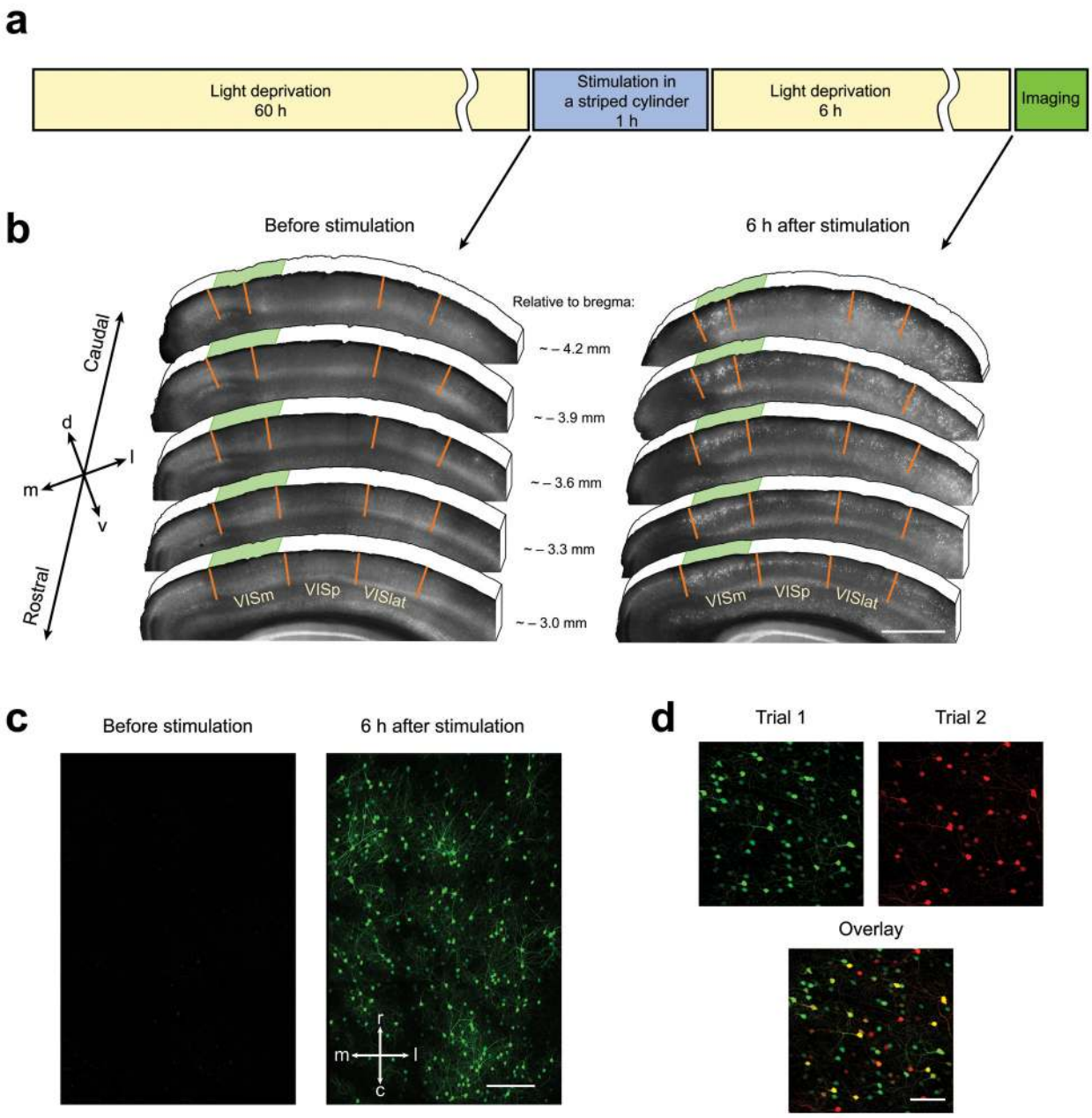

Figure 1.

Arc::dVenus expression pattern in the visual cortex following structured light stimulation. (**a**) Visual stimulation paradigm. Prior to stimulation mice were single-housed in their home cages in the dark for 60 hours. After light deprivation period mice were placed into illuminated cylinder with vertical black and white stripes for 1 hour and then transferred back into dark home cage for 6 hours until imaging. (**b**) Postmortem IHC analysis of Arc::dVenus expression in mouse visual cortex. Visual area borders are based on Allen Mouse Brain Reference Atlas (http://mouse.brain-map.org). Left panel: virtually no Arc::dVenus is present in the visual cortex at the end of 60-hour light deprivation period. Right panel: 6 hours after visual stimulation Arc::dVenus is present largely in the medial extrastiate visual cortex (VISm) and to lesser extent in the lateral extrastirate (VISlat) and primary (VISp) visual areas. Green shading indicates approximate location of the *in vivo*

imaging site shown in (**c**). Scale bar = 1000 μm. (**c**) Maximum intensity projections of *in vivo* multiphoton imaging data from the same region of medial extrastriate visual cortex after light deprivation (left panel) and 6 hours after 1-hour visual stimulation in a cylinder with vertical stripes (right panel). Image stacks were aligned using fluorescent angiogram (not shown for clarity). Scale bar = 200 μm. (**d**) Aligned maximum intensity projections of image stacks from a visual cortex region imaged in two repetitive stimulation trials. Scale bar = 100 μm.

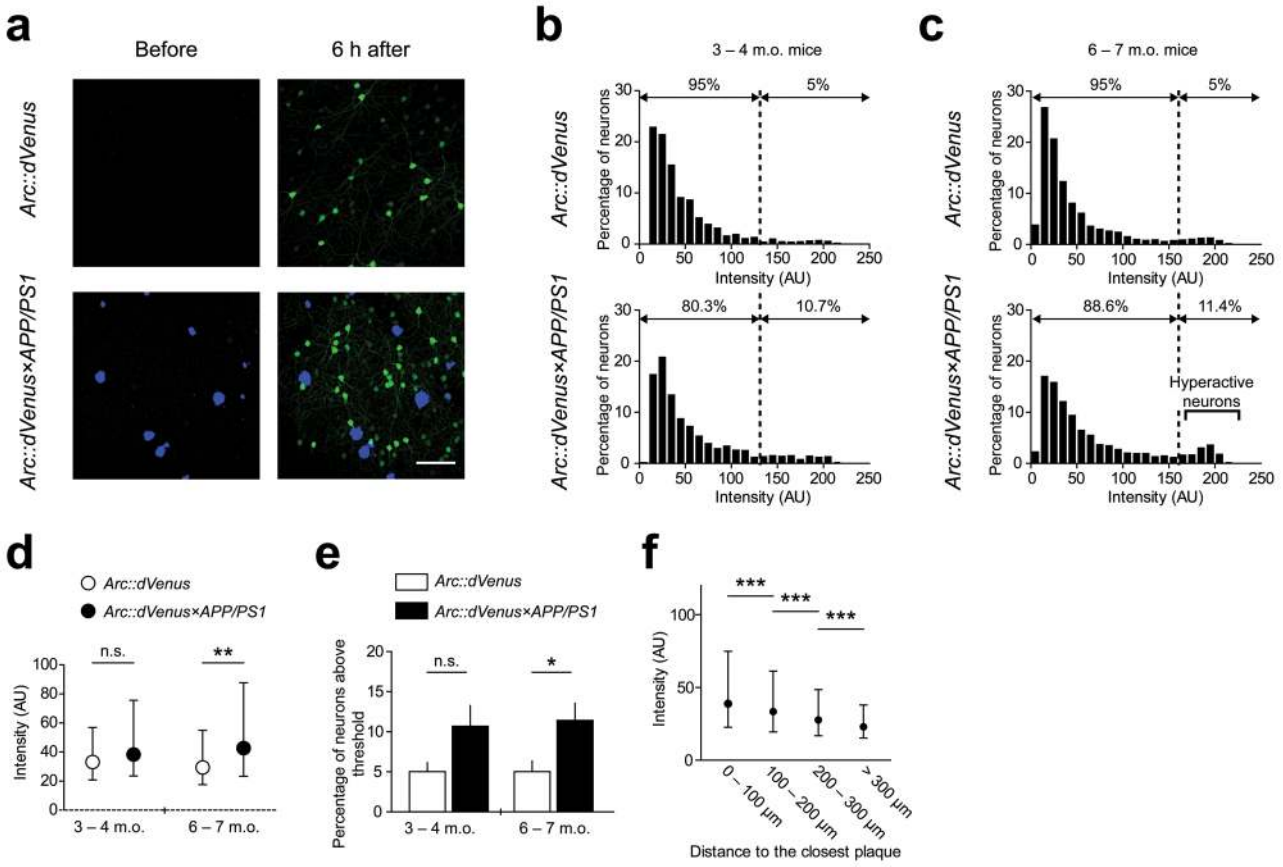

Figure 2.

Effect of amyloid plaques on stimulus-induced Arc::dVenus expression levels

(**a**) Example of maximum intensity projection of *in vivo* imaging dataset used for quantification. Blue–amyloid plaques visualized with methoxy-X04, green–Arc::dVenus fluorescence. Scale bar = 100 µm. (**b**) Frequency distribution histograms of *in vivo* activity-induced Arc::dVenus expression levels in neurons of young pre-plaque *Arc::dVenus×APP/PS1* mice (n = 4 mice, 1590 neurons; bottom panel) and control littermates (n = 4 mice, 1322 neurons; top panel). AU–arbitrary unit. (**c**) Frequency distribution histograms of *in vivo* activity-induced Arc::dVenus expression levels in neurons of aged plaque-bearing *Arc::dVenus×APP/PS1* mice (n = 8 mice, 3410 neurons; bottom panel) and control littermates (n = 8 mice, 2753 neurons; top panel). (**b**–**c**) Dotted line indicates threshold Arc::dVenus expression level separating 5% of brightest neurons in control mice. (**d**) Comparison of distributions of Arc::dVenus expression levels from (**b**) and (**c**). Distribution medians with interquartile ranges are plotted. **P < 0.01. (**e**) Mean (across mice) percentage of neurons with stimulus-induced Arc::dVenus expression levels above the threshold. Error bars represent standard error of mean (s.e.m.). *P < 0.05. (**f**) Stimulus-induced Arc::dVenus expression levels in *Arc::dVenus×APP/PS1* mice are elevated in the vicinity of amyloid plaques. Neurons were binned based on their distance to the closest amyloid plaque and the medians of Arc::dVenus expression levels are presented with interquartile ranges. N = 8 *Arc::dVenus×APP/PS1* mice, 3250 neurons; ***P < 0.001.

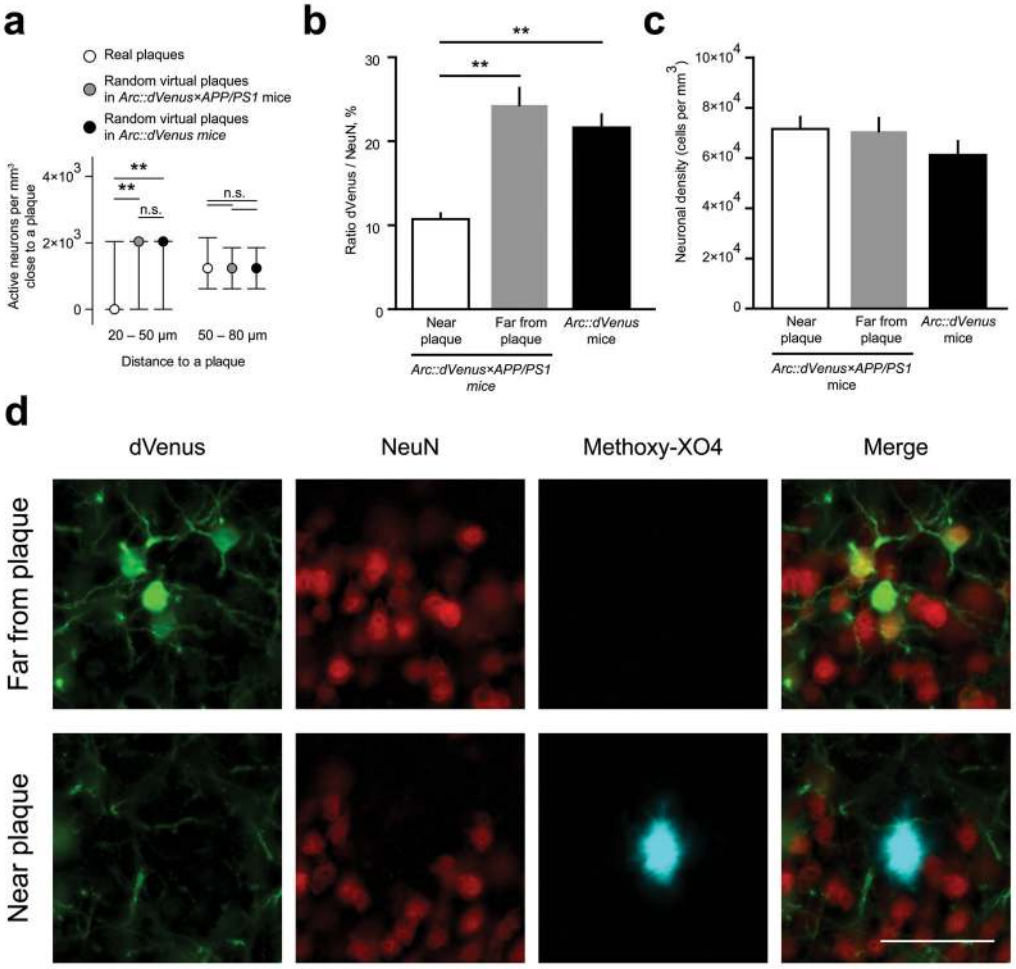

Figure 3.

Local effect of amyloid plaques on spatial distribution of Arc::dVenus-positive neurons (**a**) Number of detectable neurons following stimulation is decreased in 20–50 μm range from the plaque center and is not affected at 50–80 μm. Neuronal counts in the vicinity of real amyloid plaques (n = 204) in *Arc::dVenus×APP/PS1* mice are compared to the counts around randomly placed virtual plaques introduced into the neuronal datasets from *Arc::dVenus×APP/PS1* mice (n = 8) and *Arc::dVenus* control littermates (n = 8), normalized to the respective volumes. Data are presented as medians with interquartile ranges.**P < 0.01. (**b**) Stereological postmortem quantification reveals that the proportion of NeuN-positive neurons expressing Arc::dVenus in response to the stimulation is lower near amyloid plaques (less than 65 μm from the plaque's edge) than far from plaques (more than 65 μm in *Arc::dVenus×APP/PS1* cortex. N = 3 mice for each condition. **P < 0.01. (**c**) Density of NeuN-positive neurons near and far from plaques and in control brain. N = 3 mice for each condition. Data in (**b**–**c**) are presented as means±s.e.m. (**d**) Immunohistochemical staining of medial extrastriate visual cortex of an *Arc::dVenus×APP/PS1* mouse sacrificed 6 hours after the end of 1-hour structured visual stimulation. Green–GFP, red– NeuN, blue–amyloid plaques visualized with methoxy-X04 delivered *in vivo*. Scale bar = 50 μm.

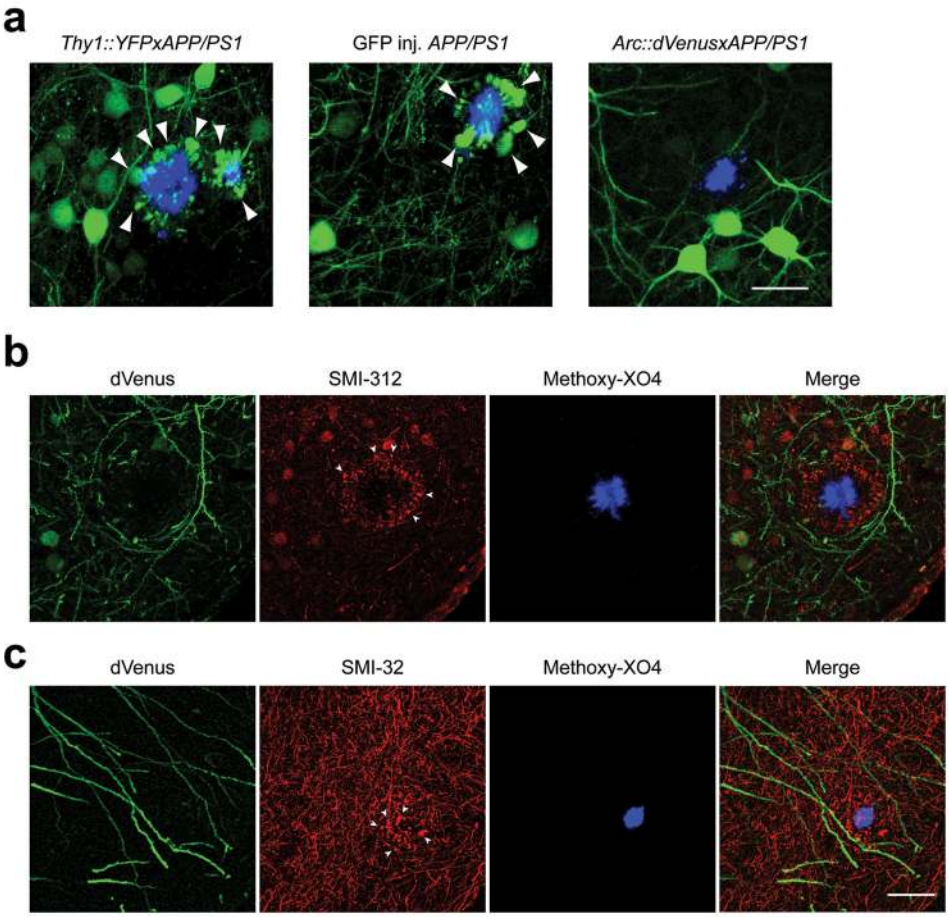

Figure 4.

Neurons with dystrophic neurites do not express Arc::dVenus in response to a stimulus. (**a**) Maximum intensity projections of *in vivo* image stack of *Thy1::YFP×APP/PS1* transgenic mouse, *APP/PS1* mouse injected with GFP AAV2 virus and *Arc::dVenus×APP/PS1* mouse 6 hours after visual stimulation. Blue–amyloid plaques visualized with methoxy-X04; green–YFP, GFP or dVenus fluorescence. Arrowheads point at YFP- and GFP-filled neuritic dystrophies characteristic for the *APP/PS1* model. Scale bar = 30 μm. (**b**,**c**) Postmortem immunostaining of *Arc::dVenus×APP/PS1* mouse brain tissue acquired 6 hours after visual stimulation for *Arc::dVenus* (with anti-GFP antibody, green channel) showed no co-localization of experience-dependent dVenus expression with either axonal (SMI-312, (**b**)) or dendritic (SMI-32, (**c**)) neurofilament staining (red channel) that typically accumulates in dystrophic axons or dendrites (arrowheads) around amyloid plaques (methoxy-X04, blue channel). Scale bar = 30 μm is shared by (**b**,**c**).

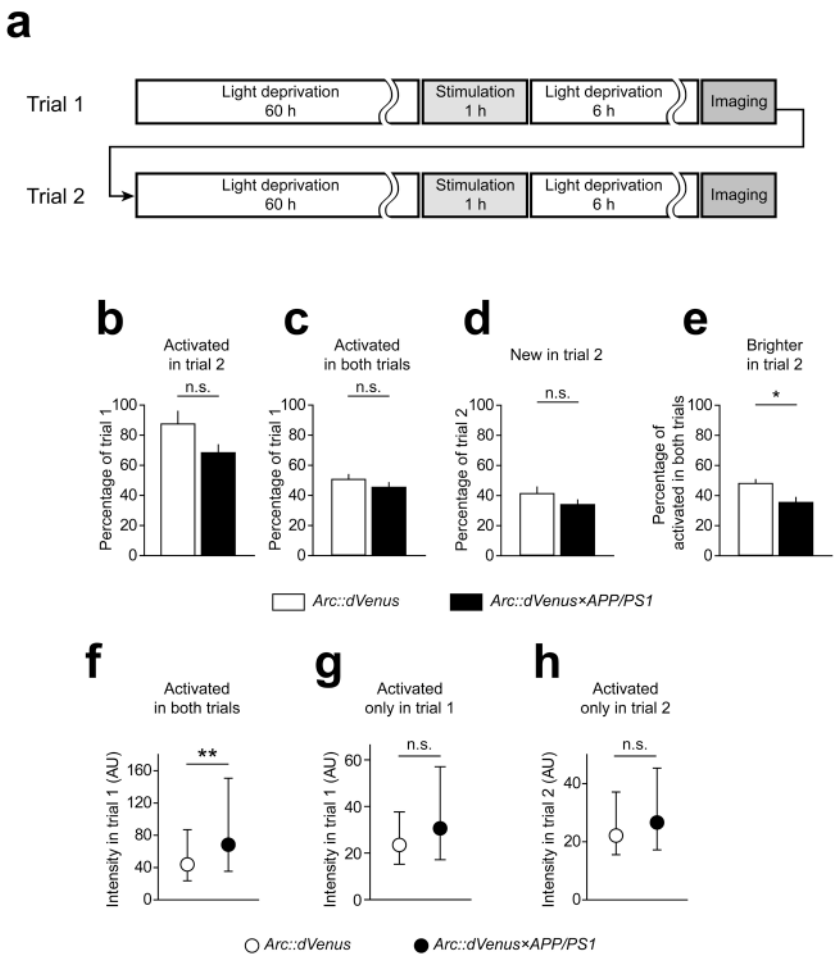

Figure 5.

Arc::dVenus expression in repetitive stimulation paradigm

(**a**) Repeated visual stimulation paradigm. Upon the completion of the first imaging session(trial 1), mice were returned to the light-proof dark enclosure for additional 60 hours until trial 2 stimulation and imaging. (**b**) Total number of neurons expressing Arc::dVenus in the second trial was lower than in the first trial, which was not affected by *APP/PS1* genotype (repeated measures two-way ANOVA: effect of trial $P < 0.01$; effect of genotype $P = 0.39$). Proportions of neurons activated in both trials (**c**) and neurons only activated in the second trial (**d**) was not changed in *Arc::dVenus×APP/PS1* mice, but the number of neurons that responded in both trials and had higher Arc::dVenus expression levels in the second trial was significantly decreased in *Arc::dVenus×APP/PS1* mice (**e**). Data in (**b**–**e**) are presented as means±s.e.m. (**f**–**h**) Differential comparison of distributions of Arc::dVenus expression levels in different population of neurons; data presented as medians with interquartile ranges. Stimulus-induced Arc::dVenus expression levels were specifically increased by amyloid plaque pathology in neurons that were activated in both trials (**f**) but not in neurons that were activated only in trial 1 (**g**) or only in trial 2 (**h**). **$P < 0.001$. In (**b**–**h**) n = 6 *Arc::dVenus* mice, n = 7 *Arc::dVenus×APP/PS1* mice.

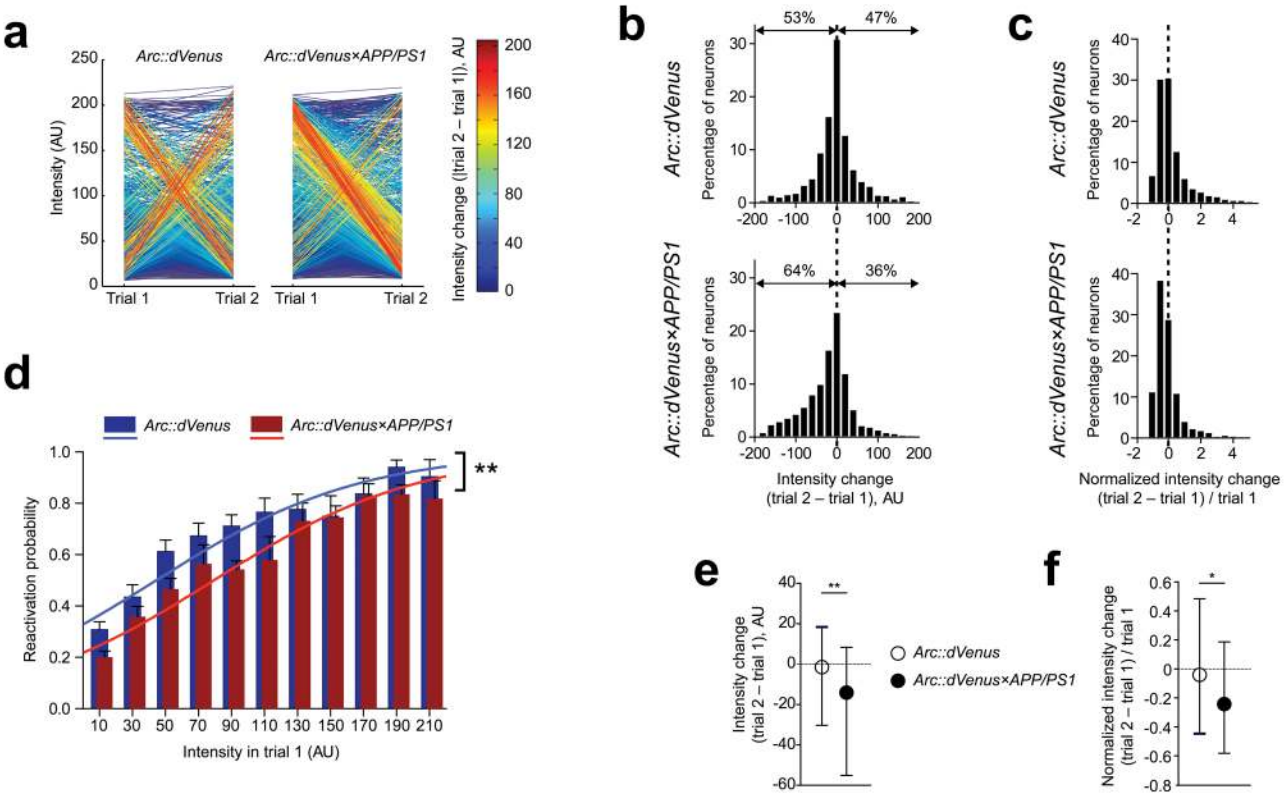

Figure 6.

Stimulus-specific Arc::dVenus expression is affected by amyloid plaque pathology

(**a**) Change of levels of visual stimulus-induced Arc::dVenus expression in two consecutive trials. Each line connects expression levels for a single neuron on trial 1 and trial 2 and is color-coded based on absolute intensity changes. In control mice (left panel) populations of neurons experiencing both maximal changes of expression levels between two trials are balanced, while in *Arc::dVenus×APP/PS1* mice (right panel) a large population of neurons hyperactive in trial 1 reactivate in trial 2 with minimal expression levels. This effect contributes to the significant negative shift of median expression levels in *Arc::dVenus×APP/PS1* mice (bottom panel on (**b**)), a distribution which is relatively symmetrical in control littermates (top panel on (**b**)). (**c**) Distributions of Arc::dVenus expression level changes normalized to trial 1 expression confirm this negative shift in intensity of reactivated neurons in *Arc::dVenus×APP/PS1* mice. (**e**, **f**) Comparison of medians of distributions presented correspondingly on (**b**) and (**c**). Data in (**e**) and (**f**) are presented as medians with interquartile ranges. *P < 0.05, **P < 0.01. (**d**) Probability of activation of a neuron in trial 2 as a function of Arc::dVenus expression level in trial 1 is reduced in *Arc::dVenus×APP/PS1* mice. Solid lines represent logistic regression model-based probabilities for *Arc::dVenus×APP/PS1* mice and control littermates. **P < 0.01. In (**a**–**f**) n = 6 *Arc::dVenus* mice, n = 7 *Arc::dVenus×APP/PS1* mice.